

Mark A. Sidebottom

Department of Mechanical
Engineering and Mechanics,
Lehigh University,
Bethlehem, PA 18015

Florian Feppon

Department of Mechanical
Engineering and Mechanics,
Lehigh University,
Bethlehem, PA 18015;
Centre de Mathématiques Appliquées,
École polytechnique,
91128 Palaiseau, France

Natasha Vermaak

Assistant Professor
Department of Mechanical
Engineering and Mechanics,
Lehigh University,
Bethlehem, PA 18015

Brandon A. Krick¹

Assistant Professor
Department of Mechanical
Engineering and Mechanics,
Lehigh University,
Bethlehem, PA 18015
e-mail: bakrick@lehigh.edu

Modeling Wear of Multimaterial Composite Surfaces

Iterative numerical wear models provide valuable insight into evolving material surfaces under abrasive wear. In this paper, a holistic numerical scheme for predicting the wear of rubbing elements in tribological systems is presented. In order to capture the wear behavior of a multimaterial surface, a finite difference model is developed. The model determines pressure and height loss along a composite surface as it slides against an abrasive compliant countersurface. Using Archard's wear law, the corresponding nodal height loss is found using the appropriate material wear rate, applied pressure, and the incremental sliding distance. This process is iterated until the surface profile reaches a steady-state profile. The steady-state is characterized by the incremental height loss at each node being nearly equivalent to the previous loss in height. Several composite topologies are investigated in order to identify key trends in geometry and material properties on wear performance. [DOI: 10.1115/1.4032823]

1 Introduction

As the demand for low wear materials grows, so does the need for accurate and fast wear predictions. The wear between contacting rubbing solids is termed abrasive sliding wear when it involves a harder material rubbed against softer materials [1–4]. Numerical analysis of wearing solids remains a critical engineering problem for design and manufacturing applications [5–15]. Iterative schemes have emerged as a convenient approach to model the wear of tribological systems. The models predict the topographical evolution of a wearing surface by integrating mechanical models with relationships between pressure, geometry, and material wear properties.

Ling pioneered the domain of physics-based models (analytical and numerical) for surface mechanics, friction, wear, and thermoelasticity [4,16–18]. Due to the complexity of many tribological systems, very few simple solutions exist to predict the lifetime of a given system. For simple mechanisms such as cylindrical bushings, tribological behavior can be predicted using analytical solutions [19–22], but more complex systems require numerical methods. Often finite element modeling (FEM) and numerical schemes are used to model surface mechanics, frictional heating and wear [5–12,23]. In many of these wear simulations, FEM models are used to calculate contact pressures, which are then used to compute wear based on Archard's wear law (wear is proportional to sliding distance and contact pressure) [1,2]. These computations can be challenging and time consuming, as systems must be remeshed and FEM calculations repeated for each wear iteration. This approach becomes even more difficult in composite material systems where more than one material is present.

Recently, a finite difference model [24] has been used to simulate the wear of multimaterial three-dimensional (3D) systems ranging from polymer composites to dinosaur teeth [25,26]. The approach is based on a two-parameter Pasternak elastic foundation wear model that has been validated and successfully used in previous numerical and experimental studies [5,14,27,28] (see Fig. 1). One advantage of this approach is that contact pressure calculations are made quasi-analytically, reducing computational costs compared to alternative methods like FEM. In particular, for a given multimaterial surface, nodal wear height and curvature are used to compute instantaneous pressure. With this pressure, local wear loss for each node is found as a function of incremental sliding distance (Δs) and the corresponding material wear rate (K). This process is repeated until the composite system reaches a steady-state configuration. Steady-state is determined when the incremental height loss at each node is constant for all nodes.

In this article, the finite difference model previously presented [24] is clarified and redefined in three dimensions and a parametric analysis is performed in order to identify key relationships between model parameters, including elastic foundation parameters (k_s and k_g) and geometric factors like area fraction and topology. The paper is organized as follows. A summary of the finite difference model previously implemented in Refs. [24–27] is presented. Then numerous steady-state wear profiles are computed as part of a parametric study. Practical applications and potential design rules based on the identified trends are discussed.

2 Wear Model Description

The linear abrasive wear model takes as input, the two-dimensional (2D) material configuration within a design domain and the corresponding material wear rate properties, as well as the initial pressure loadings in the plane (Fig. 2). The material wear rate for each node is defined as the steady-state wear rate of that

¹Corresponding author.

Contributed by the Tribology Division of ASME for publication in the JOURNAL OF TRIBOLOGY. Manuscript received July 5, 2015; final manuscript received September 22, 2015; published online July 26, 2016. Assoc. Editor: Robert L. Jackson.

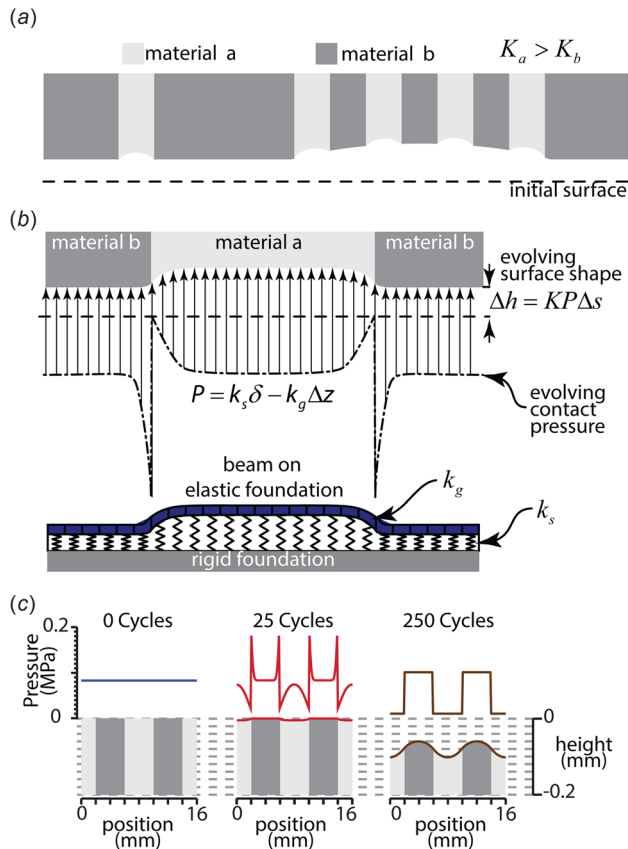


Fig. 1 Schematic of wear model that couples the evolution of contact pressure and the surface topography. (a) Nonuniform wear in multimaterial surfaces. The wear rate of material B, K_b , is less than that of material A. (b) Schematic of pressure and topography model. (c) Example evolution of contact pressure and surface topography for a bimaterial surface after 0, 25, and 250 sliding cycles.

single material in dry contact against an abrasive elastic foundation. The model uses these inputs to predict the 3D evolution of the initially flat or 2D wear surface under the initial pressure load. The initially flat surface profile evolves to a nonuniform surface topography because of differences in local wear rates. As the wear continues, the surface topography evolves toward a steady-state and the pressure profile distribution becomes uniform for each material constituent (with magnitude inversely proportional to wear rate, see Fig. 1(c)). The profile eventually reaches a steady-

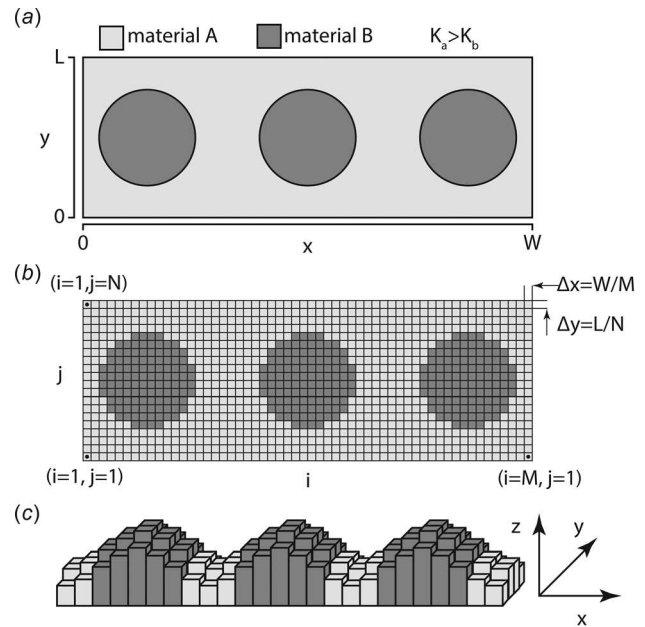


Fig. 3 (a) and (b) Simplified diagram showing the discretization of a composite surface. There are two materials (A, B) with the wear rates $K_a > K_b$ for this example. (c) Schematic worn profile.

state condition that recesses at a constant rate. This transient run-in wear behavior was experimentally observed in Refs. [24,27,29], and compared with numerical predictions of the steady-state profile. The initially uniform pressure profile evolves in a manner that depends on the local calculated curvature of the worn surface profile. In this way, the model elucidates areas of the design domain that will undergo more wear than others and how the initial geometry or configuration plays a role in the final worn surface for a given initial pressure and material distribution. The components and assumptions of the wear model are described in the following.

The model assumes that a composite material is on an elastic Pasternak foundation. The Pasternak elastic foundation model is composed of spring elements that are coupled with a bending beam element; the corresponding parameters are k_s and k_g , respectively (Fig. 2),

$$p = k_s \delta - k_g \nabla^2 z \quad (1)$$

where δ is the local deflection of the elastic foundation with respect to a moving height reference (recessing because of the

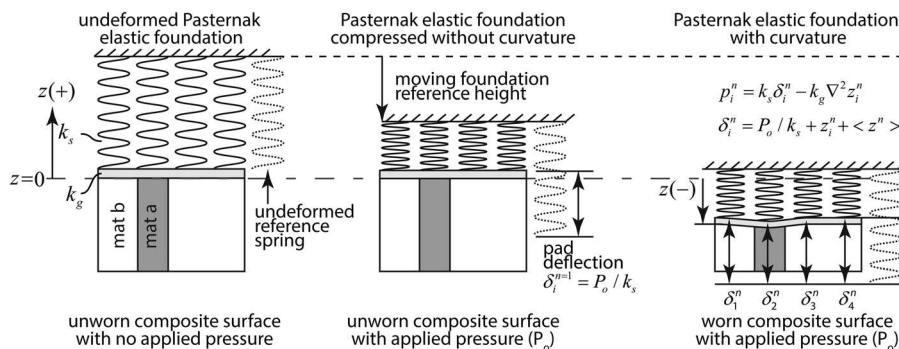


Fig. 2 Physical description of the numerical wear model. The Pasternak elastic foundation model is composed of spring elements that are coupled with a bending beam element; the corresponding parameters are k_s and k_g , respectively. The pressure applied at each node is a function of the deflection of the spring element (δ) and the local curvature ($\nabla^2 z$).

wear process), z is the surface height, and $\nabla^2 z = (\partial^2 z / \partial x^2) + (\partial^2 z / \partial y^2)$ is the Laplacian of z . The notation $\langle \cdot \rangle$ refers to an average value of a parameter. The domain, Ω , has dimensions W , width, by L , length. This domain is discretized into an $M \times N$ grid, with the pixel dimensions: $\Delta x = W/M$ and $\Delta y = L/N$ (Fig. 3). Δs is an incremental sliding distance. The iterative scheme is used to predict the shape of the evolving surface, with i, j as subscripts to denote spatial ordinates and the superscript, n , as an iteration counter. The evolving surface is then characterized by the height, $z_{i,j}^n$, of the worm profile at the position, $(i\Delta x, j\Delta y)$ of the grid and after a sliding distance, $d = n\Delta s$. Following Ref. [27], an initially flat profile is assumed and loaded with an initially uniform pressure distribution, P_0 . An additional constraint that the average pressure, $\langle p \rangle$, must remain constant over the domain, Ω , is applied [27].

Each material (“a” and “b”) has its own distinct wear rate, K_a or K_b of units (mm^3/Nm). For an initial configuration, a composite wear rate matrix is constructed, $K_{i,j}$, such that the matrix values represent nodal values of the wear rate in the domain of the sample surface. This is a known material input that also represents initial surface material configuration.

For every iteration, n , the incremental wear depth relative to the initially flat surface, Δh (mm), at a particular surface location (i, j) is calculated

$$\Delta h_{i,j}^n = p_{i,j}^n \Delta s K_{i,j} \quad (2)$$

where Δs represents the incremental sliding distance and $p_{i,j}^n$ is the evolved local pressure profile along the surface. The initial value, $p_{i,j}^{n=1}$, is the average of the known applied pressure profile, P_0 .

Equation (1) is discretized in the following way:

$$p_{i,j}^n = k_s \delta_{i,j}^n - k_g \left(\frac{z_{i+1,j}^n - 2z_{i,j}^n + z_{i-1,j}^n}{\Delta x^2} + \frac{z_{i,j+1}^n - 2z_{i,j}^n + z_{i,j-1}^n}{\Delta y^2} \right) \quad (3)$$

where $\delta_{i,j}^n$ is the deflection at iteration n on the node i, j . The previous equation, Eq. (3), assumes extension by periodicity

$$z_{N+1,j}^n = z_{1,j}^n, \quad z_{0,j}^n = z_{N,j}^n, \quad z_{i,M+1}^n = z_{i,1}^n, \quad z_{i,0}^n = z_{i,M}^n \quad (4)$$

are applied in order to ensure physical meaning at the domain boundaries in Eq. (3) for all i, j such that $1 \leq i \leq N$ and $1 \leq j \leq M$. The constraint that the average pressure must remain a constant is applied

$$P_0 = \frac{1}{MN} \sum_{i,j} p_{i,j}^n \quad (5)$$

As a result, the average of the deflection at iteration n must satisfy

$$\langle \delta_{i,j}^n \rangle = \frac{P_0}{k_s} \quad (6)$$

where the notation $\langle v \rangle$ denotes the discretized average of a matrix

$$v_{i,j} : \langle v \rangle = \frac{1}{MN} \sum_{i,j} v_{i,j}^n$$

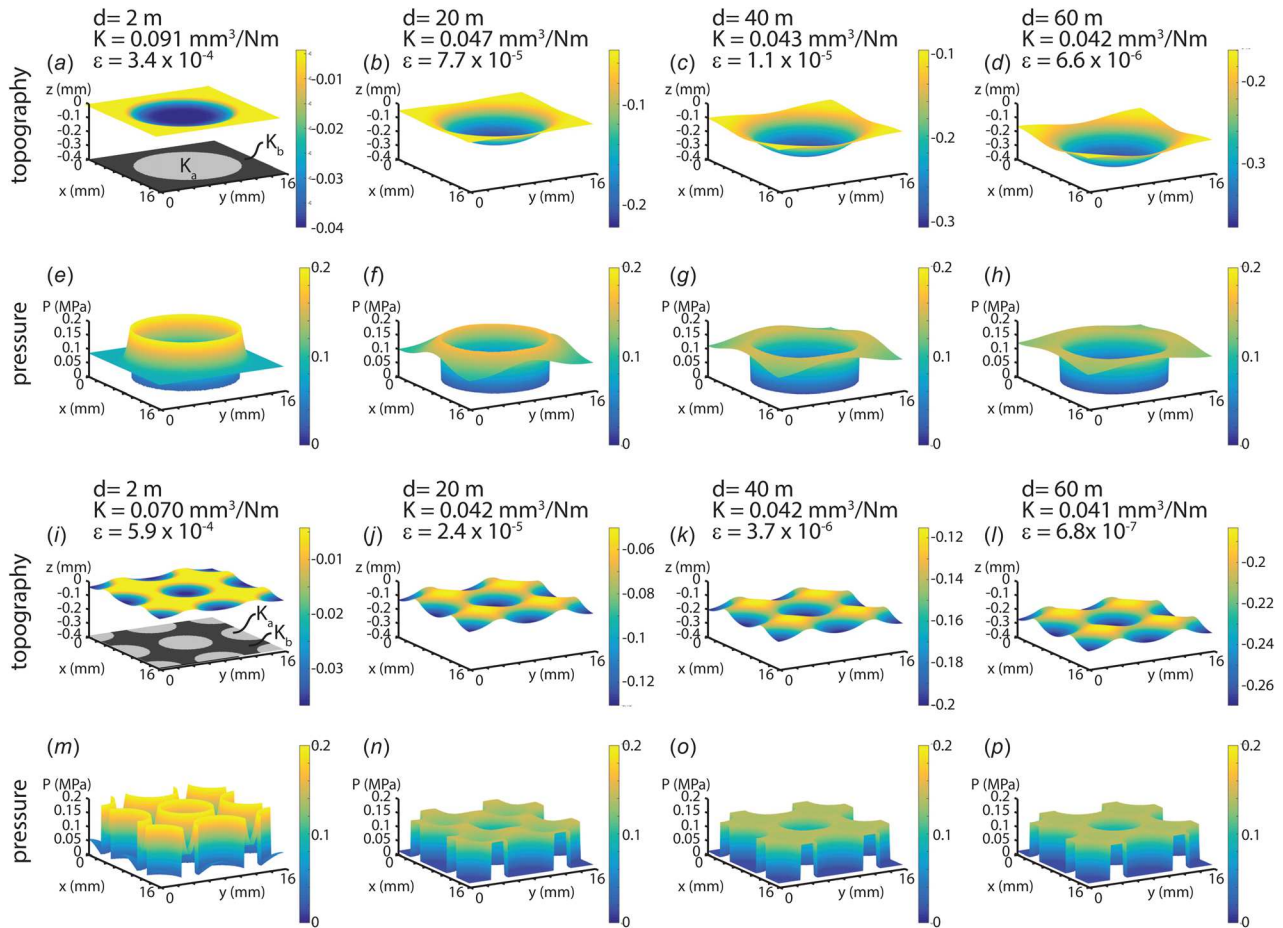


Fig. 4 Model iterations revealing evolution of topography and compressive contact pressure for small-inclusion and large-inclusion configurations with the same area fraction. $K_a = 0.25 \text{ mm}^3/\text{Nm}$, $K_b = 0.025 \text{ mm}^3/\text{Nm}$, $k_s = 0.28 \text{ N/mm}^3$, $k_g = 2.8 \text{ N/mm}$, $P = 0.083 \text{ (MPa)}$, $\Delta s = 0.002$, $A_a = 0.441 \text{ m}$. Note: Topography has fixed z-axis (not to 1:1 scale), but a changing color scale is used for ease of visualization. Pressure has a fixed axis and colorscale.

This implies that the deflection in every point must be related to the height of the profile $z_{i,j}^n$ by the relationship

$$\delta_{i,j}^n = \frac{P_0}{k_s} + z_{i,j}^n - \langle z^n \rangle \quad (7)$$

The local pressure profile evolves as follows:

$$p_{i,j}^n = P_0 + k_s(z_{i,j}^n - \langle z^n \rangle) - k_g \left(\frac{z_{i+1,j}^n - 2z_{i,j}^n + z_{i-1,j}^n}{\Delta x^2} + \frac{z_{i,j+1}^n - 2z_{i,j}^n + z_{i,j-1}^n}{\Delta y^2} \right) \quad (8)$$

Defining the wear rate coefficient as $K_{i,j} = K(i\Delta x, j\Delta y)$, then the profile at the next iteration, $z_{i,j}^{n+1}$, is updated using Archard's law ($\Delta h = pK\Delta s$)

$$z_{i,j}^{n+1} = z_{i,j}^n - p_{i,j}^n K_{i,j} \Delta s \quad (9)$$

This procedure is the one that was followed by Rowe et al. in Ref. [27] and similar schemes were also used in Refs. [5] and [24]. The procedure is iterated sufficiently long for a steady-state to be reached. The steady-state solution is determined when two successive increments, $\zeta_{i,j}^n = z_{i,j}^n - z_{i,j}^{n-1}$ and $\zeta_{i,j}^{n+1} = z_{i,j}^{n+1} - z_{i,j}^n$, have equal local wear-loss at every point, that is,

$$\max \frac{|\zeta_{i,j}^{n+1} - \zeta_{i,j}^n|}{|\zeta_{i,j}^n|} = \epsilon < \epsilon_{\text{converge}} \quad (10)$$

where $\epsilon_{\text{converge}}$ is a small parameter fixed based on desired level of precision. It has been observed previously [10,30] that instabilities can occur if Δs (Eq. (9)) is too small; this will be investigated in future work.

3 Numerical Results and Discussion

The iterative model was used to find the steady-state wear rate for varying material distributions and area fractions. In every case, a 16×16 mm domain (160×160 nodes) was modeled with the following parameters: $K_a = 0.25 \text{ mm}^3/\text{N} \cdot \text{m}$, $K_b = 0.025 \text{ mm}^3/\text{N} \cdot \text{m}$, $k_s = 0.28 \text{ N}/\text{mm}^3$, $k_g = 2.8 \text{ N}/\text{mm}$, and $P = 0.083 \text{ MPa}$. It should be noted that the wear rates of the two materials are based on epoxy ($K = 0.24 \text{ mm}^3/\text{Nm}$) and PEEK ($K = 0.019 \text{ mm}^3/\text{Nm}$) under abrasive conditions as reported by Rowe et al. [27]. They were set at exactly an order of magnitude apart to simplify comparisons and parametric evaluation of the model. Simulations were run for a minimum sliding distance of 60 m or, if additional iterations were required, until a value of epsilon less than 10^{-6} was reached. The evolution of topography and contact pressure for two different material topologies is shown in Fig. 4 for various sliding increments. These topologies consist of a matrix of material B with different size inclusions of material A (Figs. 4(a) and 4(i)). In all cases, the area fraction of material A is $A_a = 0.441$. In both cases, after 2 m of sliding distance, there is a very high pressure region near the material boundary (Figs. 4(e) and 4(m)). As the sliding distance increases, the pressure maxima at the boundary of the two materials decreases. The small-inclusion configuration's pressure profile has reached steady-state ($\epsilon < 10^{-6}$) before 60 m of sliding distance, which is illustrated by the step-function-like pressure profile (Fig. 4(p)). For the large-inclusion configuration, the pressure profile has not converged with $\epsilon < 10^{-6}$. It is still evolving after 60 m of sliding, as illustrated by the nonuniform pressure distributions over each material domain (Fig. 4(h)). This difference is reflected by the values of epsilon for the two cases (small-inclusions $\epsilon = 6.8 \times 10^{-7}$, large-inclusion $\epsilon = 6.6 \times 10^{-6}$).

The total worn volume versus sliding distance for both circle cases is shown in Fig. 5(a). In the plot, the star data markers represent the sliding distance when epsilon reduces by orders of

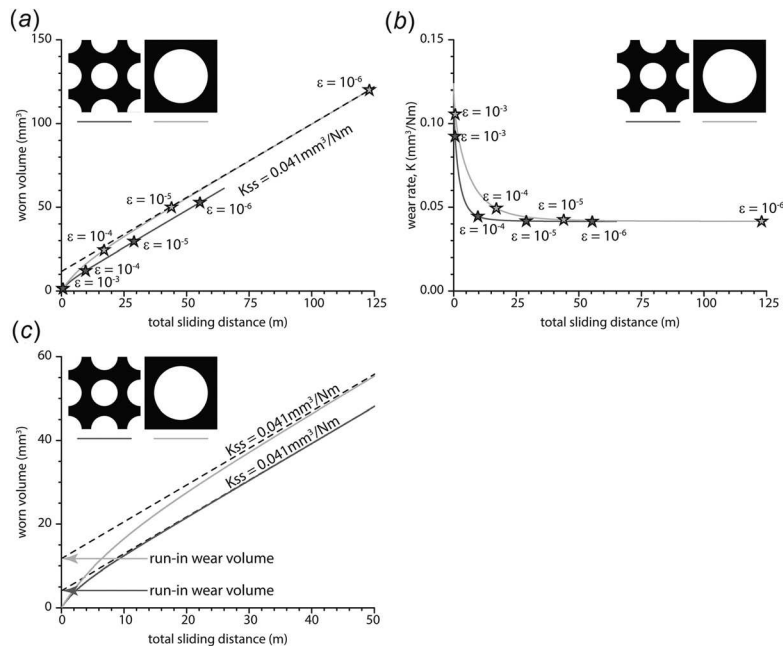
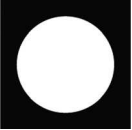
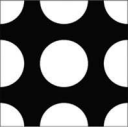


Fig. 5 Model iterations and convergence for several material topologies. (a) A comparison of two 16×16 mm material distributions with the same area fraction ($A_a = 0.441$). The more finely distributed material converges to a steady-state wear rate with less sliding distance than the single inclusion domain. (b) Current wear rate for each iteration both configurations; example values of convergence criterion (ϵ) highlighted with star data points. (c) Rescaled worn volume versus sliding distance to emphasize the difference in run-in wear volume. Note: $K_a = 0.25 \text{ mm}^3/\text{Nm}$, $K_b = 0.025 \text{ mm}^3/\text{Nm}$, $k_s = 0.28 \text{ N}/\text{mm}^3$, $k_g = 2.8 \text{ N}/\text{mm}$, $P = 0.083 \text{ MPa}$, and $\Delta s = 0.002 \text{ m}$.

Table 1 Performance analysis of the iterative scheme considering varying convergence criteria, $\epsilon_{\text{converge}}$

| | Convergence criteria ($\epsilon_{\text{converge}}$) | Sliding distance | Volume lost (mm ³) | Wear rate (mm ³ /Nm) | Percent error in wear from steady-state |
|---|---|------------------|--------------------------------|---------------------------------|---|
|  | 1×10^{-3} | 0.656 | 1.56 | 0.106 | 154 |
| | 1×10^{-4} | 17.0 | 24.5 | 0.0494 | 19.1 |
| | 1×10^{-5} | 44.0 | 49.9 | 0.0425 | 2.48 |
| | 1×10^{-6} | 123 | 120 | 0.04153 | 0.175 |
|  | 1×10^{-3} | 0.584 | 1.27 | 0.0924 | 123 |
| | 1×10^{-4} | 9.70 | 12.1 | 0.0445 | 7.39 |
| | 1×10^{-5} | 29.0 | 29.6 | 0.0417 | 0.665 |
| | 1×10^{-6} | 55.4 | 52.8 | 0.0415 | 0.0419 |

magnitude, from 10^{-3} to 10^{-6} (Fig. 5(a) and Table 1). The sliding distance to convergence for the large-inclusion distribution (123 m) was much greater than the small-circle distribution (55.4 m). Incremental wear rate versus sliding distance converges to the steady-state wear rate value of 0.041 mm³/Nm (Fig. 5(b)). The wear volume increases linearly with sliding distance at steady-state (Fig. 5(c)). A proposed metric for how effective a material distribution is at reaching steady-state wear for a given area fraction is the run-in wear, $V_{\text{run-in}}$ (Eq. (11)); the run-in wear volume is shown graphically as the y-intercept of the steady-state wear lines as they intersect the vertical axis in the worn volume and sliding distance plot in Fig. 5(c)

$$V_{\text{run-in}} = V_{\text{total}} - K_{ss} P_o W L_{ss} \quad (11)$$

where V_{total} is the total wear volume at convergence, K_{ss} is the steady-state wear rate, and d_{ss} is the sliding distance to steady-state convergence. $P_o W L$ is the total applied force over the entire surface, thus $K_{ss} P_o W L_{ss}$ is the volume that would be worn if the surface was wearing at the steady-state wear rate the entire time.

A number of numerical configurations were investigated (Fig. 6). These show how material area fractions (ranging from $A_a = 0.01$ to 0.994) influence the total wear rate (Fig. 6(a)), steady-state wear rate (Fig. 6(b)), and run-in wear volume

(Fig. 6(c)). The simpler topologies (without finely distributed inclusions) had greater total wear rates (Fig. 6(a)); their steady-state wear rates (Fig. 6(b)) depend only on the area fraction. As was noted by Rowe et al. [27], the steady-state wear rate for this model follows an inverse rule of mixtures relationship based on the individual material wear rates and the material area fractions see Eq. (12). This

$$K_{ss} = \frac{K_a}{A_a + \frac{K_a}{K_b} (1 - A_a)} \quad (12)$$

This can be extended to a composite surface with more than two wear rates in the following equation:

$$K_{ss} = \left(\frac{1}{MN} \sum_{i=1}^M \sum_{j=1}^N K_{ij}^{-1} \right)^{-1} \quad (13)$$

where K_{ij} is the wear rate at each pixel i, j over the $M \times N$ domain.

The effect of material distribution on run-in volume is shown in Fig. 6(c). Larger run-in wear volumes are undesirable, as a large amount of run-in could lead to premature failure of a composite

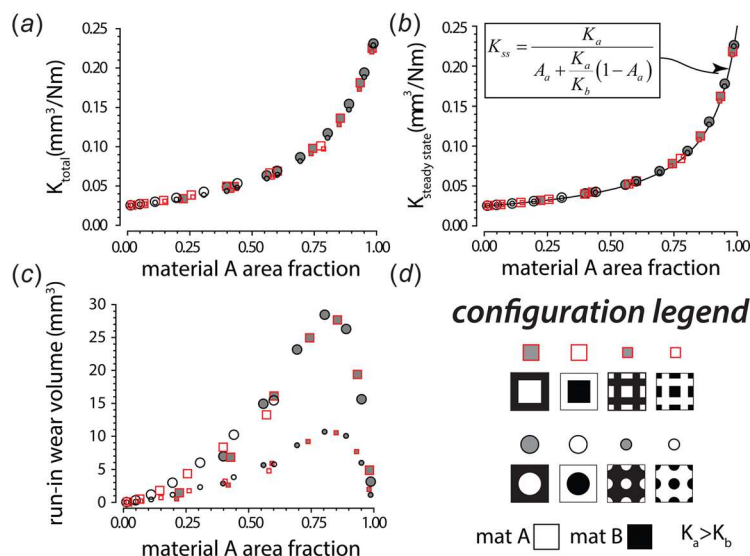
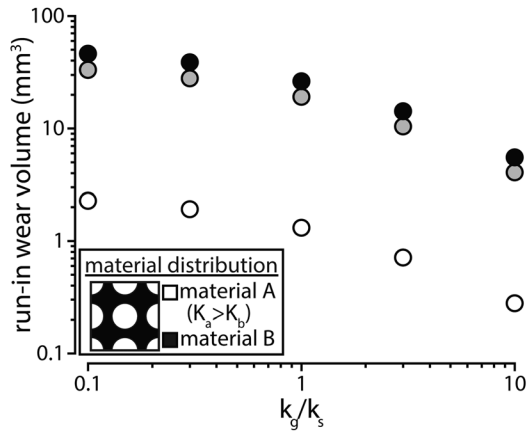


Fig. 6 Model results for various area fractions of material A (ranging from 0.01 to 0.99). A 16×16 mm domain (160×160 nodes) was modeled with the following parameters: $K_a = 0.25$ mm³/Nm, $K_b = 0.025$ mm³/Nm, $k_s = 0.28$ N/mm³, $k_g = 2.8$ N/mm, $P = 0.083$ MPa, and $\Delta s = 0.0002$ m. Total wear rate (a), steady-state wear rate (b), and run-in volume (c) are shown for various material configurations (d).



| | K_a/K_b | K_a (mm ³ /Nm) | K_b (mm ³ /Nm) |
|---|-----------|-----------------------------|-----------------------------|
| ○ | 1.5 | 5.30×10^{-2} | 3.54×10^{-2} |
| ● | 10 | 2.50×10^{-1} | 2.50×10^{-2} |
| ● | 100 | 2.34×10^0 | 2.34×10^{-2} |

Legend: model parameters

Fig. 7 Effect of k_g/k_s and K_a/K_b ratios on run-in wear volume. Run-in wear volume at convergence ($\epsilon_{\text{converge}} = 10^{-6}$) plotted for various k_g/k_s ratios (ranging from 0.1 to 10, with $k_s = 0.28 \text{ N/mm}^3$ fixed) and K_a/K_b ratios (ranging from 1.5 to 100; selected to have a constant steady-state wear rate of $K_{ss} = 4.14 \times 10^{-2} \text{ mm}^3/\text{Nm}$ for $A_a = 0.441$). A $16 \times 16 \text{ mm}$ domain (160×160 nodes) was modeled with the $P = 0.083 \text{ MPa}$. Inset in bottom left corner shows the material distribution used for all simulations.

part. Generally, larger domains that have less well-dispersed inclusions have higher run-in volumes. Based on these parametric studies for bimaterial composites, it is expected that the finer the dispersion of inclusions, the better the run-in wear characteristics will be.

The run-in wear volume is also a function of the elastic foundation parameters. A parametric analysis was performed to study the effect of k_g/k_s and K_a/K_b ratios on run-in wear volume at convergence ($\epsilon_{\text{converge}} = 10^{-6}$). k_g/k_s was varied from 0.1 to 10, by modifying k_g for a fixed $k_s = 0.28 \text{ N/mm}^3$. The ratio K_a/K_b was varied from 1.5 to 100 by solving for K_a and K_b for a fixed area fraction $A_a = 0.441$ and steady-state wear rate $K_{ss} = 4.14 \times 10^{-2} \text{ mm}^3/\text{Nm}$; this is based off of the steady-state wear rate from the area fraction study (see Fig. 6). A $16 \times 16 \text{ mm}$ domain (160×160 nodes) was modeled with the $P = 0.083 \text{ MPa}$. For a given topology, as the bending term, k_g , increases the run-in wear volume decreases (see Fig. 7). This is because the k_g term represents the countersurfaces resistance to bending or curvature. This results in lower peak-to-peak surface topography (between high and low wearing materials) which manifests as lower run-in volume. In this model, the steady-state wear rate is independent of k_g and k_s .

4 Conclusions

An improved finite difference formulation for the wear of multimaterial composite surfaces was presented that allows the designer to investigate the influence of key material and geometric parameters in the performance of engineered wear surfaces. The developments include a clarified elastic foundation model, formalized periodic boundary conditions, and a convergence criterion. The model was used to predict the wear of numerous surface topographies. This model is shown to be a promising component of mechanical design for many applications ranging from tribological (e.g., developing optimal composites for wear) to manufacturing (e.g., designing surface topographies through topology).

Acknowledgment

This material is based upon work supported by the National Science Foundation under Grant No. 1538125. This work was funded by the Lehigh University Faculty Innovation Grant. The authors gratefully acknowledge Dr. Georgios Michailidis (SIMaP-Université de Grenoble, INPG, France) for his valuable advice on this project.

Nomenclature

- A_a = area fraction of material a
- d_{ss} = the sliding distance at steady-state or convergence
- i = column index (x -direction)
- j = row index (y -direction)
- K = wear rate
- k_g = elastic foundation bending stiffness
- k_s = elastic foundation normal stiffness
- K_a = wear rate of material a
- K_b = wear rate of material b
- K_{ss} = steady-state wear rate
- L = model surface length (y -dimension)
- M = total number of columns in discretized surface (x -direction)
- n = iteration number (sliding distance index)
- N = total number of rows in discretized surface (y -direction)
- p = local pressure
- P_o = nominal applied contact pressure
- $V_{\text{run-in}}$ = run-in volume
- V_{total} = total wear volume
- W = model surface width (x -dimension)
- z = surface height
- δ = local deflection of elastic foundation
- δx = pixel dimension in x direction
- δy = pixel dimension in y direction
- Δh = local change in height caused by wear
- Δs = incremental slip distance
- $\epsilon_{\text{converge}}$ = model convergence factor
- ζ = incremental change in height for iteration of model

References

- [1] Archard, J., and Hirst, W., 1956, "The Wear of Metals Under Unlubricated Conditions," *Proc. R. Soc. London, Ser. A*, **236**(1206), pp. 397–410.
- [2] Archard, J. F., 1953, "Contact and Rubbing of Flat Surfaces," *J. Appl. Phys.*, **24**(8), pp. 981–988.
- [3] Hatchett, C., 1803, "Experiments and Observations on the Various Alloys, on the Specific Gravity, and on the Comparative Wear of Gold," *Philos. Trans. R. Soc. London*, **93**, pp. 43–194.
- [4] Ling, F., 1959, "A Quasi-Iterative Method for Computing Interface Temperature Distributions," *Z. Angew. Math. Phys.*, **10**(5), pp. 461–476.
- [5] Pödra, P., and Andersson, S., 1997, "Wear Simulation With the Winkler Surface Model," *Wear*, **207**(1), pp. 79–85.
- [6] Pödra, P., and Andersson, S., 1999, "Finite Element Analysis Wear Simulation of a Conical Spinning Contact Considering Surface Topography," *Wear*, **224**(1), pp. 13–21.
- [7] Podra, P., and Andersson, S., 1999, "Simulating Sliding Wear With Finite Element Method," *Tribol. Int.*, **32**(2), pp. 71–81.
- [8] Kim, N. H., Won, D., Burris, D., Holtkamp, B., Gessel, G. R., Swanson, P., and Sawyer, W. G., 2005, "Finite Element Analysis and Experiments of Metal/Metal Wear in Oscillatory Contacts," *Wear*, **258**(11), pp. 1787–1793.
- [9] Mukras, S., Kim, N. H., Mauntler, N. A., Schmitz, T. L., and Sawyer, W. G., 2010, "Analysis of Planar Multibody Systems With Revolute Joint Wear," *Wear*, **268**(5), pp. 643–652.
- [10] Mukras, S., Kim, N. H., Sawyer, W. G., Jackson, D. B., and Bergquist, L. W., 2009, "Numerical Integration Schemes and Parallel Computation for Wear Prediction Using Finite Element Method," *Wear*, **266**(7), pp. 822–831.
- [11] Lengiewicz, J., and Stupkiewicz, S., 2013, "Efficient Model of Evolution of Wear in Quasi-Steady-State Sliding Contacts," *Wear*, **303**(1), pp. 611–621.
- [12] Fregly, B. J., Sawyer, W. G., Harman, M. K., and Banks, S. A., 2005, "Computational Wear Prediction of a Total Knee Replacement From In Vivo Kinematics," *J. Biomech.*, **38**(2), pp. 305–314.
- [13] Chongyi, C., Chengguo, W., and Ying, J., 2010, "Study on Numerical Method to Predict Wheel/Rail Profile Evolution Due to Wear," *Wear*, **269**(3), pp. 167–173.

- [14] Telliskivi, T., 2004, "Simulation of Wear in a Rolling–Sliding Contact by a Semi-Winkler Model and the Archard's Wear Law," *Wear*, **256**(7), pp. 817–831.
- [15] Sawyer, W. G., Argibay, N., Burris, D. L., and Krick, B. A., 2014, "Mechanistic Studies in Friction and Wear of Bulk Materials," *Annu. Rev. Mater. Res.*, **44**(1), pp. 395–427.
- [16] Batra, S., and Ling, F., 1967, "On Deformation Friction and Interface Shear Stress in Viscoelastic-Elastic Layered System Under a Moving Load," *ASLE Trans.*, **10**(3), pp. 294–301.
- [17] Ling, F., and Pu, S., 1964, "Probable Interface Temperatures of Solids in Sliding Contact," *Wear*, **7**(1), pp. 23–34.
- [18] Kennedy, F., and Ling, F., 1974, "A Thermal, Thermoelastic, and Wear Simulation of a High-Energy Sliding Contact Problem," *ASME J. Tribol.*, **96**(3), pp. 497–505.
- [19] Dickrell, D., Dooner, D., and Sawyer, W., 2003, "The Evolution of Geometry for a Wearing Circular Cam: Analytical and Computer Simulation With Comparison to Experiment," *ASME J. Tribol.*, **125**(1), pp. 187–192.
- [20] Blanchet, T., 1997, "The Interaction of Wear and Dynamics of a Simple Mechanism," *ASME J. Tribol.*, **119**(3), pp. 597–599.
- [21] Dickrell, D. J., and Sawyer, W. G., 2004, "Evolution of Wear in a Two-Dimensional Bushing," *Tribol. Trans.*, **47**(2), pp. 257–262.
- [22] Sawyer, W. G., 2001, "Wear Predictions for a Simple-Cam Including the Coupled Evolution of Wear and Load," *Lubr. Eng.*, **57**(9), pp. 31–36.
- [23] Ling, F. F., Lai, W. M., and Lucca, D. A., 2002, *Fundamentals of Surface Mechanics: With Applications*, Springer Science & Business Media, New York.
- [24] Sawyer, W., 2004, "Surface Shape and Contact Pressure Evolution in Two Component Surfaces: Application to Copper Chemical Mechanical Polishing," *Tribol. Lett.*, **17**(2), pp. 139–145.
- [25] Erickson, G. M., Krick, B. A., Hamilton, M., Bourne, G. R., Norell, M. A., Lilleodden, E., and Sawyer, W. G., 2012, "Complex Dental Structure and Wear Biomechanics in Hadrosaurid Dinosaurs," *Science*, **338**(6103), pp. 98–101.
- [26] Erickson, G. M., Sidebottom, M. A., Kay, D. L., Turner, K. T., Ip, N., Norell, M. A., Sawyer, W. G., and Krick, B. A., 2015, "Wear Biomechanics in the Slicing Dentition of the Giant Horned Dinosaur Triceratops," *Sci. Adv.*, **1**(5), p. e1500055.
- [27] Rowe, K. G., Erickson, G. M., Sawyer, W. G., and Krick, B. A., 2014, "Evolution in Surfaces: Interaction of Topography With Contact Pressure During Wear of Composites Including Dinosaur Dentition," *Tribol. Lett.*, **54**(3), pp. 249–255.
- [28] Flodin, A., and Andersson, S., 1997, "Simulation of Mild Wear in Spur Gears," *Wear*, **207**(1), pp. 16–23.
- [29] Lee, G. Y., Dharan, C., and Ritchie, R. O., 2002, "A Physically-Based Abrasive Wear Model for Composite Materials," *Wear*, **252**(3), pp. 322–331.
- [30] Johansson, L., 1994, "Numerical Simulation of Contact Pressure Evolution in Fretting," *ASME J. Tribol.*, **116**(2), pp. 247–254.